HOSTED BY

ELSEVIER

CrossMark

Available online at www.sciencedirect.com

ScienceDirect

Progress in Natural Science: Materials International 25 (2015) 419–424

Progress in Natural Science Materials International

www.elsevier.com/locate/pnsmi
www.sciencedirect.com

Original Research

Structural and dielectric properties of doped ferrite nanomaterials suitable for microwave and biomedical applications

Imran Sadiq[a,*], Shahzad Naseem[a], Muhammad Naeem Ashiq[b], M.A. Khan[c], Shanawer Niaz[d], M.U. Rana[a]

[a]Centre of Excellence in Solid State Physics, University of the Punjab, Lahore, Pakistan
[b]Institute of Chemical Sciences, Bahauddin Zakariya University, Multan 60800, Pakistan
[c]Department of Physics, BUITEMS, Quetta, Pakistan
[d]Department of Physics, University of Sargodha, Sargodha, Pakistan

Received 14 May 2015; accepted 31 July 2015
Available online 31 October 2015

Abstract

The sol–gel auto-combustion method was adopted to synthesize nanomaterials of single-phase X-type hexagonal ferrites with the composition of $Sr_{2-x}Gd_xNi_2Fe_{28-y}Cd_yO_{46}$ ($x=0.00$, 0.02, 0.04, 0.06, 0.08, 0.10 and $y=0$, 0.1, 0.2, 0.3, 0.4, 0.5). The structural properties were carried out by XRD analysis and the lattice parameters show variation with the doping of Gd–Cd. The average particle size measured by TEM was in the range of 8–10 nm which is beneficial in obtaining suitable signal-to-noise ratio in recording media and biomedical applications. The room temperature resistivity enhanced with the increase of the dopant concentration. The increase in resistivity indicates that the synthesized materials can be considered good for the formation of the multilayer chip inductors (MLCIs) as well as for the reduction of eddy current losses. The dielectric constant decreased with the increase in the frequency which is the general reported trend of the hexagonal ferrites and can be explained on the basis of Koop's theory and Maxwell–Wagner polarization-model. The abnormal dielectric behavior indicates the formation of small polarons in the material. The maximum value of tangent loss at low frequencies reflects the application of these materials in medium frequency devices (MF).

Keywords: Sol–gel; Nanocrystalline materials; Thermal properties; Electrical properties; Dielectric properties

1. Introduction

With the rapid development of modern communication technique and electronic devices in recent years, the electromagnetic and microwave radiation pollutions are becoming a serious problem. As a result, more and more researches are focusing on developing antiradiation materials and microwave absorbing materials [1–5]. Magnetoplumbite hexaferrites are suitable for electromagnetic interference suppression and radar absorbent materials due to their strong magnetic losses at gigahertz frequency [6]. For the hexagonal structure, there are six possible different types namely M, W, X, Y, Z and U. All the complex hexaferrites are structurally different with respect to the combinations of S ($2MFe_2O_4$), R (Ba/Sr Fe_6O_{11}) and/or T ($(Ba/Sr)_2$ Fe_8O_{14}) blocks while the Gibbs free energies of their formation are similar, and the thermodynamic conditions for their formation are also similar. Therefore, a local inhomogeneity and/or non-stoichiometry in the reaction mixtures with the stoichiometry of a particular hexaferrite (e.g.,W-hexaferrite=(RSS)$_2$) can result in the formation of another hexaferrite with a slightly different combination of structural blocks (e.g., X-hexaferrite=(RS)2S) [7–8]. Among all the hexagonal ferrites, the X-type hexaferrites with low coercivity and high saturation magnetization can be considered good for microwave absorption properties and the preparation of single phase X-type hexagonal ferrite requires very high temperature which is the challenging task [14]. Furthermore, the rare earth

*Corresponding author. Tel.: +92 42 99231136.
E-mail address: khanphysics@yahoo.com (I. Sadiq).

http://dx.doi.org/10.1016/j.pnsc.2015.09.011

elements substituted materials exhibit a variety of effects originating from the coupling between two spin subsystems. As the transition elements are very less anisotropic than the rare earth elements, the orientations of the hexagonal ferrites can be controlled with the substitution of rare earth elements in pure ferrites, which affects the magnetic, optical and elastic properties significantly [9–10].

Many researchers have synthesized and characterized the rare earth elements doped nanoferrites. Ashiq et al. [8] have reported the structural, electrical and magnetic properties of Gd–Sn substituted $Sr_{1-x}Gd_xFe_{12-y}Sn_yO_{19}$ (where $x=0.00$, 0.025, 0.05, 0.075, 0.1 and $y=0.00$, 0.25, 0.5, 0.75, 1) prepared by the sol–gel combustion method. The average crystallite size lies in the range of 19–42 nm. DC electrical resistivity shows the transition of metal to semiconductor with temperature, and the magnetic properties of the samples decreased with additives. The citrate-precursor method was adopted to synthesize the rare earth element La^{3+} substituted $Sr_{1-x}La_xFe_{12}O_{19}$ ($x=0$, 0.08, 0.13, 0.18) M-type hexaferrites by Want et al. [11]. The dielectric, conducting and impedance properties were measured as a function of frequency and additive concentration in the frequency ranges of 20 Hz to 3 MHz. The decrease in saturation magnetization and increase in coercivity were observed with the increase of La^{3+} concentration. However, the structural, electrical and dielectric properties of Gd–Cd doped X-type hexagonal ferrites have seldom been reported.

In the present work, an attempt has been made to synthesize the single phase $Sr_{2-x}Gd_xNi_2Fe_{28-y}Cd_yO_{46}$ ($x=0.00$, 0.02, 0.04, 0.06, 0.08, 0.10 and $y=0$, 0.1, 0.2, 0.3, 0.4, 0.5) X-type hexagonal nanoferrites by using the sol–gel method, and the effect of Gd–Cd substitution on the structural, electrical and dielectric properties of X-type hexagonal nanoferrites has been investigated.

2. Experimental procedure

The polycrystalline X-type hexaferrites and its derivatives with composition of $Sr_{2-x}Gd_xNi_2Fe_{28-y}Cd_yO_{46}$ ($x=0.00$, 0.02, 0.04, 0.06, 0.08, 0.10 and $y=0$, 0.1, 0.2, 0.3, 0.4, 0.5) were prepared by the sol–gel method. The stoichiometric ratios of raw materials $Sr(No_3)_2$, $Cd(No_3)_2$, $NiCl_2\cdot 6H_2O$, Gd_2O_3, Iron nitrate, Citric Acid were mixed in deionized water. The gel was attained by stirring the solution at 80 °C. The gel was burnt at 400 °C for 1 h and finally sintered at 1250 °C for 6 h to attain the required phase. The powder was then pressed into pellets at a pressure of ~30 KN using Paul-Otto Weber hydraulic press by using Polyvinyl alcohol as binder.

The thermal analysis to conform the temperature at which required phase can be obtained was carried out by the Mettler Toledo TGA/DSC 1 STAR^e system equipped with Nitrogen gas. The crystalline phase after heat treatment was identified by using a Schimadzu X-Ray diffractometer equipped with Cu-Kα radiations ($\lambda=1.5406$ Å). The particle morphology was examined by JEOL JSM-6500F field emission scanning electron microscopy and TECNAI F20 Phillips High Resolution Transmission Electron Microscopy. The electrical properties were measured by a two probe method, using source meter

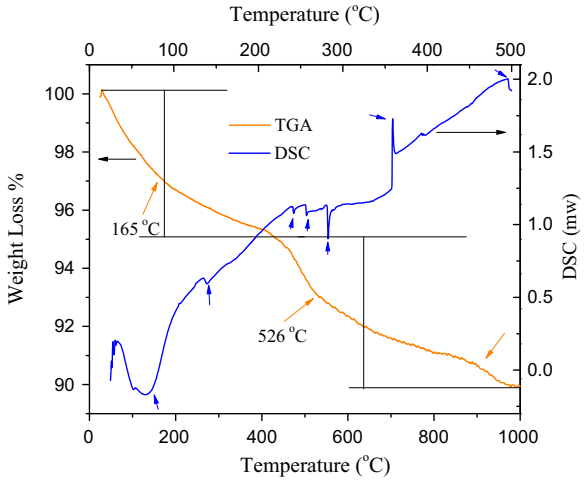

Fig. 1. (a) Thermogravimetric analysis curve for the precursor pre-sintered at 400 °C and (b) differential scanning calorimetric curve of the as synthesized precursor.

model Keithly 2400. The dielectric properties have been measured by LCR Meter. The dielectric constant was measured by using formula $\varepsilon=Cd/A\varepsilon_o$ where C is the capacitance in Farad, ε_o is the permittivity of free space (8.85×10^{-12} F m^{-1}), A is the area of cross section of flat surface of the pellet and d is the pellet thickness.

3. Results and discussion

3.1. Thermal analysis

Fig. 1(a) shows the thermogravimetric analysis of pre-sintered precursor at 400 °C for 1 h. The thermogravimetric curve can be subdivided into two endothermic peaks and an exothermic peak in the end. The endothermic peak in the temperature ranges of 120–235 °C shows the weight loss which can be attributed to the dehydration of absorbed water by the pre-sintered precursor. For the second endothermic peak, a sharp weight loss can be observed in the temperature range of 490–565 °C, which shows the oxidation of organic impurities and formation of metal oxides. The broad exothermic peak in the end of the curve shows the formation of hexagonal structure [12]. The differential scanning calorimetric curve indicates that the sample experiences the strong endothermic and exothermic changes, which may be attributed to the dehydration of water, decomposition of organic compounds and formation of metal oxides.

3.2. Structural properties

XRD patterns of X-type hexagonal ferrites sintered at 1250 °C for 6 h are shown in Fig. 2. Hexagonal single phase can be confirmed from the XRD patterns. Lattice parameters a (Å) and c (Å) were calculated by using formula;

$$\frac{1}{d_{hkl}^2}=\frac{4\left(h^2+hk+k^2\right)}{3a^2}+\frac{l^2}{c^2} \quad (1)$$

where d_{hkl} is the d-spacing of the lines in the XRD pattern and h, k and l are the corresponding Miller indices.

The unit cell volume was calculated by using following formula

$$V = a^2 c \sin 120^\circ \quad (2)$$

where "a" and "c" are lattice constants.

The unit cell volume increases with the Gd–Cd concentration up to $x=0.08$ and then decreases.

The X ray density was measured by following equation.

$$D_x = \frac{3M}{NV} \quad (3)$$

where M is the molar mass, N is the Avogadro's number and V is the volume of the unit cell.

The bulk density was measured by following relation;

$$D = \frac{m}{\pi h r^2} \quad (4)$$

where m is mass, r is the radius and h is the thickness of pellet.

The porosity was measured by using the formula of

$$P = 1 - \frac{D}{D_x} \quad (5)$$

where D and D_x are the bulk and X-rays densities, respectively.

The values of lattice constants a (Å) and c (Å), cell volume, bulk and X-ray density and porosity are listed in Table 1. Fig. 3 shows the variation of lattice constants a (Å), c (Å) and cell volume with dopants Gd–Cd. It can be seen clearly that the value of a (Å) increased slightly with dopant concentration up to $x=0.08$, $y=0.4$ and then decreased. The value of c (Å) decreased with dopant concentration up to $x=0.08$, $y=0.4$ and then increased. The unit cell volume shows the similar behavior as lattice constant a (Å). This may be due to difference in the ionic radii of Sr^{2+} (1.12 Å) and Gd^{3+} (0.938 Å). Since Sr^{2+} lies in R block so, the substitution of Sr^{2+} by Gd^{3+} decreases the distance among the layers. The substitution of Cd^{2+} (0.97 Å) by Fe^{3+} (0.645 Å) may also change the lattice parameter. The overall effect of substitution of dopants Gd–Cd results in the distortion of the unit cell. Fig. 4 shows the variation of X-ray density, bulk density and porosity with dopants Gd–Cd concentration. The porosity increased up to $x=0.04$, $y=0.2$ and then decreased. The decrease in porosity was due to negative microstrain which produces the compressive stress in the lattice, and the increase in porosity was due to the collection of small vacancies together to form the large vacancy [13].

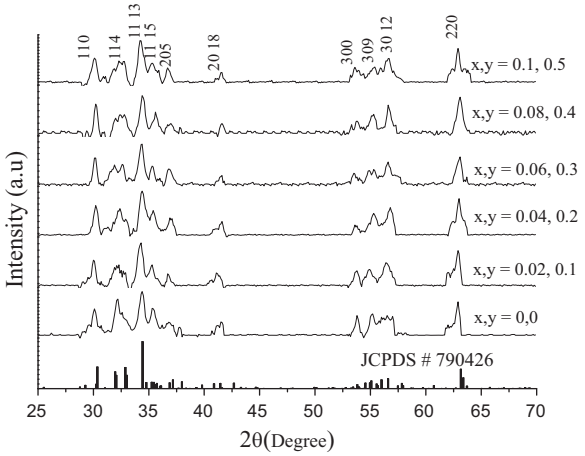

Fig. 2. XRD patterns of $Sr_{2-x}Gd_xNi_2Fe_{28-y}Cd_yO_{46}$ ($x=0.00$, 0.02, 0.04, 0.06, 0.08, 0.10 and $y=0$, 0.1, 0.2, 0.3, 0.4, 0.5) at 1250 °C for 6 h.

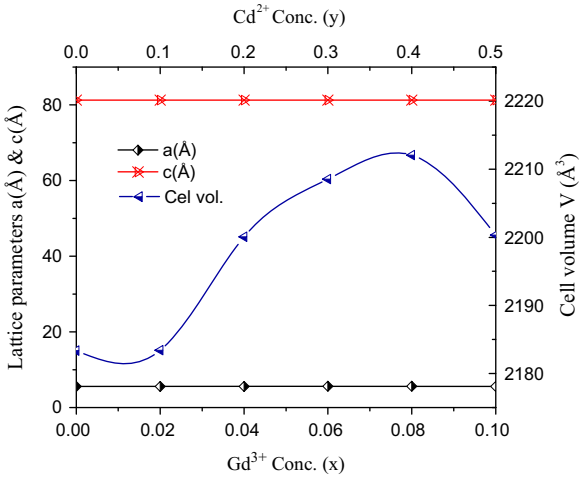

Fig. 3. Variation of lattice constants a (Å), c (Å) and unit cell volume with Gd^{3+} concentration (x) and Cd^{2+} concentration (y).

Table 1
Lattice parameters, cell volume, X-ray density, bulk density, porosity and resistivity of $Sr_{2-x}Gd_xNi_2Fe_{28-y}Cd_yO_{46}$ ($x=0.00$, 0.02, 0.04, 0.06, 0.08, 0.10 and $y=0$, 0.1, 0.2, 0.3, 0.4, 0.5) at 1250 °C for 6 h.

Parameters	$x,y=$ 0,0	$x,y=0.02,0.1$	$x,y=0.04,0.2$	$x,y=0.06,0.3$	$x,y=0.08,0.4$	$x,y=0.1,0.5$
lattice constant a (Å)	5.5699	5.5701	5.5920	5.6031	5.6076	5.5920
lattice constant c (Å)	81.265	81.262	81.243	81.235	81.235	81.258
unit cell volume (Å)^3	2183.37	2183.40	2200.06	2208.53	2212.08	2200.33
X rays density D_x (g/cm^3)	5.916	5.932	5.903	5.89	5.90	5.95
bulk density D (g/cm^3)	3.593	3.555	2.71	3.13	3.5	3.63
porosity P	0.392	0.4	0.54	0.46	0.40	0.38
resistivity (Ω cm) × 10^8	1.3	5.2	7.6	10.0	28.0	13.0

3.3. Grain morphology

Fig. 5(a) shows the HRSEM micrograph of $Sr_{1.96}Gd_{0.04}Ni_2Fe_{27.80}Cd_{0.2}O_{46}$ of X-type hexagonal ferrites. It can be seen easily that the very small nanoparticles agglomerate to form the big grains of platelet like structure. It is inferred that the hexagonal platelets could be randomly dispersed or oriented to give the high magnetic permeability for the incident microwaves, which is good for microwave absorption properties, and hence the present synthesized material can be the better candidate to be used as microwave absorbing material [14]. TEM analysis (Fig. 5b) shows a big nanograin composed of small nanoparticles. HRTEM micrograph (Fig. 5c) shows that the very small nanoparticles arranged in regular manner with high uniformity. The average particle size lies in the range of 8–10 nm. The DLS (Dynamic Light scattering) studies also show the average particle size in the range of 10 nm approximately. The use of magnetic nanoparticles is being intensively increased in biomedical application, such as, MRI contrast agent, Hyperthermia, target drug delivery and cellular imaging [14], and therefore present synthesized nano-sized hexagonal ferrites can be an important candidate to be used in biomedical applications. The interplaner spacing (*d* spacing) of the lattice fringes is 0.291 nm and 0.174 nm shown in Fig. 5 (d), which agrees well with the {110} and {300} lattice planes respectively of the hexagonal ferrites [15].

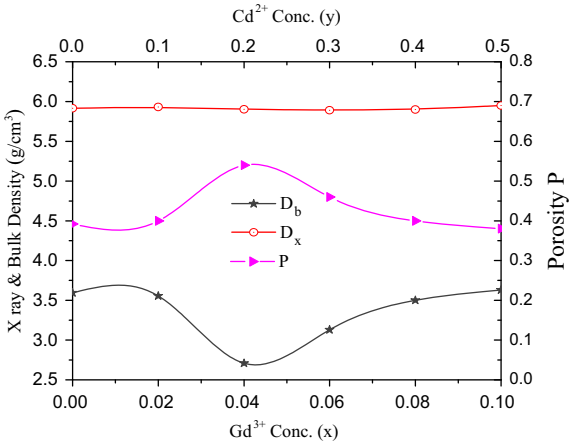

Fig. 4. Variation of the bulk and X-rays densities and porosity with Gd^{3+} concentration (*x*) and Cd^{2+} concentration (*y*).

3.4. Electrical properties

Room temperature electrical resistivity was measured for all the samples $Sr_{2-x}Gd_xNi_2Fe_{28-y}Cd_yO_{46}$ ($x=0.00$, 0.02, 0.04,

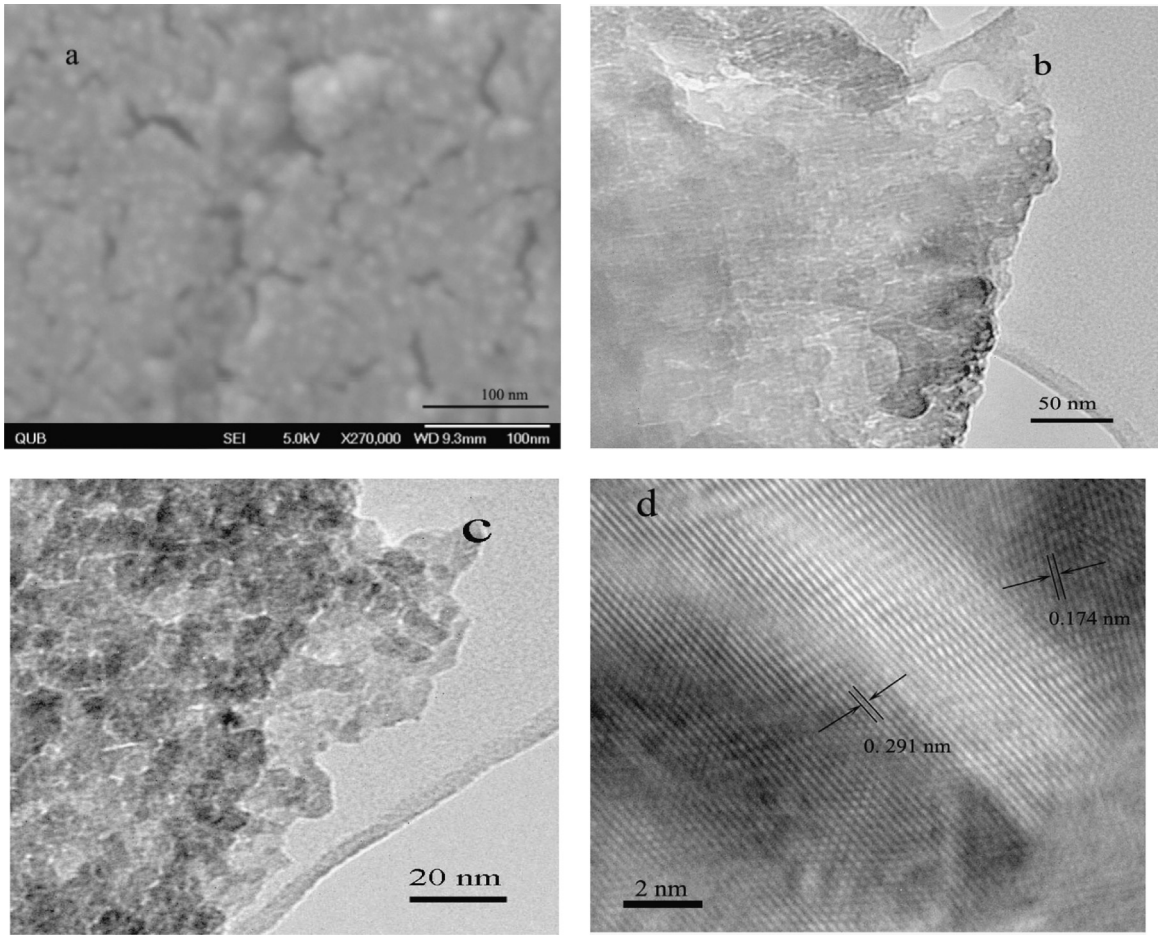

Fig. 5. HRSEM (a) TEM (b) and HRTEM (c–d) micrograph for $Sr_{1.96}Gd_{0.04}Ni_2Fe_{27.80}Cd_{0.2}O_{46}$.

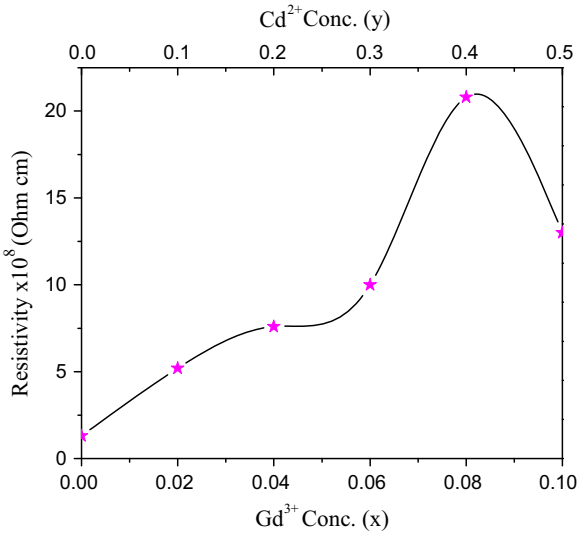

Fig. 6. Variation of resistivity (ρ) with Gd^{3+} (x) and Cd^{2+} (y) concentration.

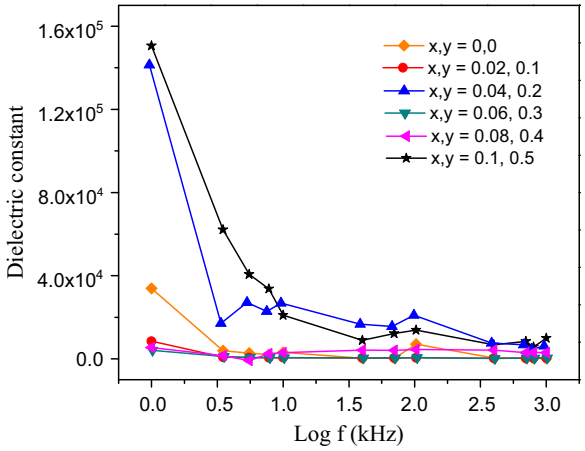

Fig. 7. Variation of the dielectric constant of all Gd–Cd concentrations with frequency.

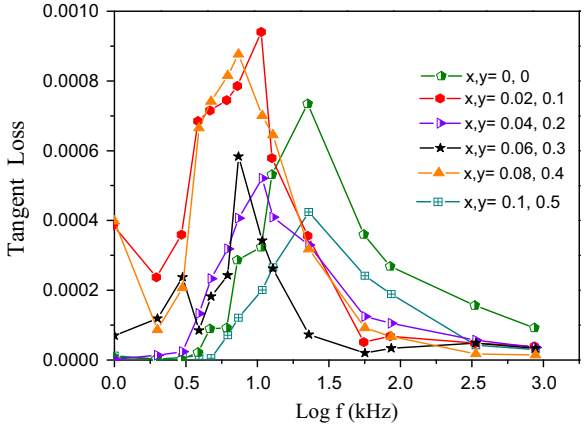

Fig. 8. Variation of the tangent loss of different Gd–Cd contents with frequency.

0.06, 0.08, 0.10 and $y=0$, 0.1, 0.2, 0.3, 0.4, 0.5) in the voltage range of 0–200 V, and the values are listed in Table 1. Fig. 6 shows the variation of electrical resistivity with Gd–Cd concentration in the voltage range of 0–200 V. Electrical resistivity of ferrites doped with Gd–Cd has greater resistivity than the undopped ferrites. It can be observed that electrical resistivity increased with dopant concentration up to $x=0.08$, $y=0.4$ and then decreased. The increase in the resistivity can be explained on the basis of site occupation of divalent Cd^{2+} ion. Kenji et al. [16] reported that the divalent ions usually occupy the octahedral sites in the R-block. The occupation of divalent Cd^{2+} ions to octahedral sites results the decrease in the number of Fe^{3+} ions at that sites, which cause the decrease in the hopping rate. And hence the conductivity decreases and the resistivity increases. The increase in the resistivity in present case indicates the occupation of octahedral sites by divalent Cd^{2+} ions. The increase in resistivity may also be due to the fact that Gd^{3+} ($134\times10^{-6}\ \Omega$ cm) is more resistive than Sr^{2+} ($21.5\times10^{-6}\ \Omega$ cm) at room temperature [17]. It can be seen that the room temperature resistivity varies in the order of $\sim10^{9}\ \Omega$ cm, which can be a good material for eddy current losses and microwave devices. Pullar et al. [14] reported that the material with high electrical resistivity has capability of rapid alignment of domains in response to high frequency magnetic field, which is a good condition for microwave absorption properties. The present investigated material with high enough resistivity is suitable for being used as microwave absorbing material. The increase in resistivity with Gd–Cd substitution makes this material suitable for the formation of the multilayer chip inductors (MLCIs).

3.5. Dielectric properties

The dielectric property is a very important characteristic of hexagonal ferrites which manifestly depends on the various factors e.g. method of preparation, sintering temperature and good selection of additive materials. Fig. 7 shows the variation of dielectric constant with the frequency of all the samples. The overall trend of the dielectric constant decreases with the frequency which is generally the characteristic of the ferrites and Orthoferrite materials [18,19]. This behavior of dielectric constant with the frequency can be explained on the basis of Maxwell–Wagner polarization model [20,21] which states that the conductivity and the dielectric ions have the same root of origin, behavior of charge carriers, the hopping between Fe^{3+} and Fe^{2+} ions. At low frequencies, the hopping frequency of charge carriers follows the applied field, which results in the increase in the dielectric constant. But at higher frequencies, the hopping frequency of charge carriers lags behind the applied field and hence the dielectric constant decreases due to random dipolar orientation. The dielectric constant behavior with the frequency can also be described on the basis of Koop's phenomenological model [22]. The variation of tangent loss with the increase of frequency of all the samples can be seen in Fig. 8. The tangent loss shows the abnormal dielectric behavior for all the samples because of the dielectric relaxation peaks. This behavior can be explained by Rezlescu model [23] which states that the dielectric relaxation peaks may be produced due to collective contribution

of P type and n type charge carriers. Bao et al. [24] reported that not only the n-type charge carriers but small polarons produced in the material also contributes to the polarization, which leads the abnormal dielectric behavior. The formation of small polarons is probable in solids due to the large coupling constant and narrow conduction band [25]. Furthermore, the formation of the relaxation peak can be attributed to the fact that the hopping frequency of localized charge carriers becomes nearly equal to the externally applied frequency, and the resonance occurs, which leads to the formation of relaxation peak. The high frequency properties and resonance losses in the form of heat make this material useful for medical applications. The maximum value of tangent loss at low frequencies makes this material beneficial in medium frequency devices (MF).

4. Conclusions

The sol–gel method provides a convenient way to prepare single phase X-type hexaferrites. The doping of Gd–Cd contents leads the change in the lattice parameters. The average particle size of the present investigated material lies in the range of 8–10 nm, which is confirmed by TEM analysis and makes this material useful for biomedical applications. The electrical resistivity lies in the order of $\sim 10^9\ \Omega$ cm, which can be a good material for eddy current losses. These materials can also be considered good for the formation of multilayer chip inductors (MLCIs). The dielectric constant has high value at low frequency and decreases rapidly with the increase of frequency, and this behavior agrees well with the Koop's phenomenological model and Maxwell–Wagner polarization model. The abnormal dielectric behavior indicates the formation of small polarons in the material.

Acknowledgments

One of author (Imran Sadiq) is thankful to the Higher Education Commission of Pakistan for the financial support “Indigenous 5000 fellowship program grant no. 20-1515/R&D/09-8049” in this project. The authors appreciate the support of Prof. Dr. Evgeny Rebrov, Queens University Belfast, Uk for providing HRTEM facilities.

References

[1] R.S. Alam, M. Moradi, M. Rostami, H. Nikmanesh, R. Moayedi, Y. Bai, J. Magn. Magn. Mater. 381 (2015) 1–9.
[2] F. Wan, F. Luo, Y. Mu, Z. Zeng, W. Zhou, J. Ceram. Int. 41 (2015) 9957–9965.
[3] Y. Köseoğlu, J. Magn. Magn. Mater. 373 (2015) 195–199.
[4] X. Shen, F. Song, X. Yang, Z. Wang, M. Jing, Y. Wang, J. Alloy. Compd. 621 (2015) 146–153.
[5] J. Shen, J. Feng, L. Li, G. Tong, Y. He, J. Alloy. Compd. 632 (2015) 490–499.
[6] X.G. Huang, J. Chen, J. Zhang, L.X. Wang, Q.T. Zhang, J. Alloy. Compd. 506 (2010) 347.
[7] E. Pollert, Crystal chemistry of magnetic oxides part 2: hexagonal ferrites, Prog. Cryst. Growth Charact. 11 (1985) 155–205.
[8] M.N. Ashiq, S. Shakoor, M.N. Haq, M.F. Warsi, I. Ali, I. Shakir, J. Magn. Magn. Mater. 374 (2015) 173–178.
[9] S. Artyukhin, M. Mostovoy, N.P. Jensen, D. Le, K. Prokes, V.G.d. Paula, H.N. Bordallo, A. Maljuk, S. Landsgesell, H. Ryll, B. Klemke, S. Paeckel, Klaus Kiefer, Kim Lefmann, L.T. Kuhn, D.N. Argyriou, J. Nat. Mater. 11 (2012) 694–699, http://dx.doi.org/10.1038/nmat3358.
[10] L. Wang, J. Zhang, Q. Zhang, N. Xu, J. Song, J. Magn. Magn. Mater. 377 (2015) 362–367.
[11] B. Want, B.H. Bhat, B.Z. Ahmad, J. Alloy. Compd. 627 (2015) 78–84.
[12] Z. Haijun, L. Zhiochao, Y. Xi, Z. Liangying, W. Mingzhong, J. Mater. Res. Bull. 38 (2003) 363.
[13] M.A. Ahmed, N. Okasha, R.M. Kershi, J. Phys. B 405 (2010) 3223.
[14] Robert C. Pullar, J. Prog. Mater. Sci. 57 (2012) 1191–1334.
[15] M.J. Molaei, A. Ataie, S. Raygan, S.J. Picken, E. Mendes, F.D. Tichelaar, J. Power Tech. 221 (2012) 292.
[16] K. Kamishima, N. Hosaka, K. Kakizaki, N. Hiratsuka, J. Appl. Phys. 109 (2011) 013904.
[17] C. Kittle, An introduction to Solid State Physics, 5th ed., Wiley, New York, 1196.
[18] M.A. El-Hiti, J. Phys. III 6 (1996) 1307.
[19] A.V.R. Reddy, G.R. Mohan, D. Ravinder, B.S. Boyanar, J. Mater. Sci. 34 (1999) 3169.
[20] J.C. Maxwell, A Treatise on Electricity and Magnetism, Oxford, New York, 1954.
[21] K.W. Wagner, J. Ann. Phys. 40 (1913) 817.
[22] C.G. Koops, J. Phys. Rev. 83 (1951) 817.
[23] N. Rezlescue, E. Rezlescu, Phys. Status Solidi A 23 (1974) 575.
[24] J. Bao, J. Zhou, Z. Yue, L. Li, Z. Gui, J. Magn. Magn. Mater. 250 (2002) 131.
[25] Y. Purushotham, P.V. Reddy, Int. J. Mod. Phys. B 10 (1996) 319.